A neuromechanical model and kinematic analyses for *Drosophila* larval crawling based on physical measurements

Xiyang Sun[a], Yingtao Liu[b], Chang Liu[c], Koichi Mayumi[c], Kohzo Ito[c], Akinao Nose[a,b], Hiroshi Kohsaka[a,*]

[a] Department of Complexity Science and Engineering, Graduate School of Frontier Science, the University of Tokyo, 5-1-5 Kashiwanoha, Kashiwa, 277-8561 Chiba, Japan

[b] Department of Physics, Graduate School of Science, the University of Tokyo, 7-3-1 Hongo, Bunkyo-ku, 133-0033 Tokyo, Japan

[c] Department of Advanced Materials Science, Graduate School of Frontier Science, the University of Tokyo, 5-1-5 Kashiwanoha, Kashiwa, 277-8561 Chiba, Japan

* For correspondence: (kohsaka@edu.k.u-tokyo.ac.jp, +81-04-7136-3922)

Abstract

Animal locomotion requires dynamic interactions between neural circuits, muscles, and surrounding environments. In contrast to intensive studies on neural circuits, the neuromechanical basis for animal behaviour remains unclear due to the lack of information on the physical properties of animals. Here, taking *Drosophila* larvae as a model system, we proposed an integrated neuromechanical model based on physical measurements. The physical parameters were obtained by a stress-relaxation assay, and the neural circuit motif was extracted from a chain of excitatory and inhibitory interneurons, which was identified previously by connectomics. Based on the model, we systematically performed perturbation analyses on the parameters in the model to study their kinematic effects on locomotion performance. We found that modification of most of the parameters in the simulation could increase the speed of locomotion. Our physical measurement and modelling would provide a new framework for neural circuit studies and soft robot engineering.

Introduction

Many animals have a soft body. Compared to animals with hard skeletons, soft-bodied animals possess high flexibility in motion and can move adaptively in complicated environments (Berrigan and Pepin, 1995; Quillin, 1999). This flexibility of soft-bodied animals suggests that output from neural circuits is not the sole determinant for locomotion. The physical properties of animals such as stiffness and viscosity should also be involved in the dynamics of locomotion (Berrigan and Pepin, 1995; Nishikawa et al., 2007; Tytell et al., 2011). Although the neural circuits for animal behaviour have been studied intensively and comprehensively, the mechanical properties of soft-bodied animals are less examined (Daun et al., 2009; Nishikawa et al., 2007). Due to the lack of physical measurements of genetically tractable soft-bodied animals, the neuromechanical basis of controlling animal motion, such as locomotion speed, remains unclear (Tytell et al., 2011).

Here, we use larvae of the fruit fly, *Drosophila melanogaster*, as a model of a soft-bodied organism to examine the neural and physical mechanisms in locomotion. *Drosophila* larvae are a useful model animal to investigate neural circuits by virtue of their genetic accessibility and the long-term accumulation of anatomical and developmental studies (Kohsaka et al., 2017). In addition, the recent advent of optogenetics and connectomics allows us to analyse neural circuits of larvae at a single cell level (Fushiki et al., 2016; Kohsaka et al., 2012), which gives us a chance to develop a neuromechanical model based on biological evidence. The *Drosophila* larva possesses a hydrostatic skeleton, supported by the fluid pressure (Fox et al., 2006). The body consists of three thoracic (T1-T3) and nine abdominal (A1-A9) segments (Gjorgjieva et al., 2013; Lahiri et al., 2011). Along the anteroposterior axis, the segmental cuticle and musculature are almost organised repetitively, especially in the abdominal segments (Ross et al., 2015).

In the repertoire of fly larval locomotion, we focus on the predominant one: forward crawling behaviour. Forward crawling consists of repeated cycles of motion called stride (Berrigan and Pepin, 1995; Heckscher et al., 2012). Each stride has two phases: 1) the visceral piston phase, where the head, tail and gut move forward together before other tissues (Ross et al., 2015); 2) the wave phase, where the contraction wave propagates from the posterior to anterior segments, with the head and tail anchored (Heckscher et al., 2012). Several interneurons for forward crawling have been identified (Itakura et al., 2015; Kohsaka et al., 2014; Yoshikawa et al., 2016; Zwart et al., 2016). Among them, the A27h premotor neuron was shown to be rhythmically active during forward but not backward locomotion (Clark et al., 2018; Fushiki et al., 2016; Kohsaka et al., 2017). Sensory feedback (Hughes and Thomas, 2007) and motor unit (Inada et al., 2011) are also critical to ensure successful wave propagation. All these biological evidences can provide hints for mathematical modelling, whether mechanical or neural (Gjorgjieva et al., 2013; Loveless et al., 2019; Pehlevan et al., 2016; Ross et al., 2015). However, previous models adopted a chain of excitatory and inhibitory neurons in the CNS to generate propagation of neural activity, which

has not yet been identified in the larval CNS (Gjorgjieva et al., 2013). In addition, neuromechanical models in previous studies were mainly based on theoretical general assumptions (Pehlevan et al., 2016; Ross et al., 2015).

In this study, we developed a novel neuromechanical model based on physical measurements of larvae and previous neural circuit studies. Based on this model, we examined the dependency of the speed of locomotion on neuromechanical parameters. We first measured the segmental dynamics of forward crawling in the third-instar larvae. Then to obtain kinetics information, we performed the stress-relaxation test on larvae and calculated viscoelastic coefficients. We found that the properties of the larval body were described better by the standard linear solid (SLS) model than by previous mechanical models. For measurement of muscle contraction force in intact larvae, we combined force measurement using a tensile tester and optogenetic activation. Based on these physical parameters and a neural circuit motif reported previously, we built a neuromechanical model for larval locomotion. This model can describe the kinematic measurement of crawling. In addition, the modelling mimics larval crawling in low-friction conditions, which we measured using high-density liquid. After establishing the model, we systematically performed perturbation analyses. By changing parameters in the model, we calculated changes in the locomotion patterns and analysed the kinematic mechanisms. By these analyses, we found that the speed of locomotion could be boosted by modifying most of the parameters in the simulation. The submaximal nature of speed implies the existence of additional factors to limit the speed of locomotion. In sum, we built a novel neuromechanical model for larval crawling based on novel physical measurements of soft-bodied larvae and previous genetic studies of neural circuits. Simulation analyses of this model proposed a submaximal nature of crawling speed. Our physical measurement and modelling method provide a new framework for neural circuit studies and soft robot engineering.

Results

Segmental kinematics of crawling behaviour in third-instar larvae

In this study, we report physical mechanisms in segmental kinematics of *Drosophila* larval crawling. We used third-instar larvae because their size (about 4 mm in length) is large enough to measure physical properties as a soft material. While previous studies examined the first- or second- instar *Drosophila* larvae and characterized the segmental kinematics (Berni, 2015; Heckscher et al., 2012; Lahiri et al., 2011; Vaadia et al., 2019; Zarin et al., 2019), crawling behaviour in the third-instar larvae had not been investigated at a segmental scale, but at a scale of the entire body (Berrigan and Pepin, 1995; Green et al., 1983; Hughes and Thomas, 2007; Kohsaka et al., 2014). Thus, we examined the motion of freely moving third-instar larvae and extended previous findings on segmental kinematics. To reliably trace the segmental boundaries of larvae, we expressed a GFP-tagged coagulation protein Fondue, which accumulates at the muscle attachment sites (Green et al., 2016). We acquired time-lapse fluorescence images from the dorsal side of the larvae where longitudinal muscles span single segments. From these fluorescence images, the segmental boundaries in thoracic (T1-T3) and abdominal (A1-A8) segments were identified (Figure 1A). We analysed the propagation of segmental contraction along the axis of the body (Figure 1B). The average intersegmental phase lag, which is the time period between peaks of muscle contraction of neighbouring segments, is about one-tenth of the stride cycles per segment (10.4$\pm$1.3 % (n=3)), which is consistent with observations in first-instar larvae (Heckscher et al., 2012). The speed of forward crawling in the third instar was 0.78$\pm$ 0.16 mm/s (n = 4). Meanwhile, the segmental dynamics are almost repetitive over segments (segmental length range: 0.18$\pm$0.05 mm~0.45$\pm$0.04 mm, from T2 to A8) (Figure 1C and Supplementary Figure 1) (Heckscher et al., 2012; Ross et al., 2015), suggesting that the physical structure of larvae can be modelled as a repetition of a single module. Thus, we obtained kinematic parameters for free moving third-instar larvae for the following physical kinetic analysis.

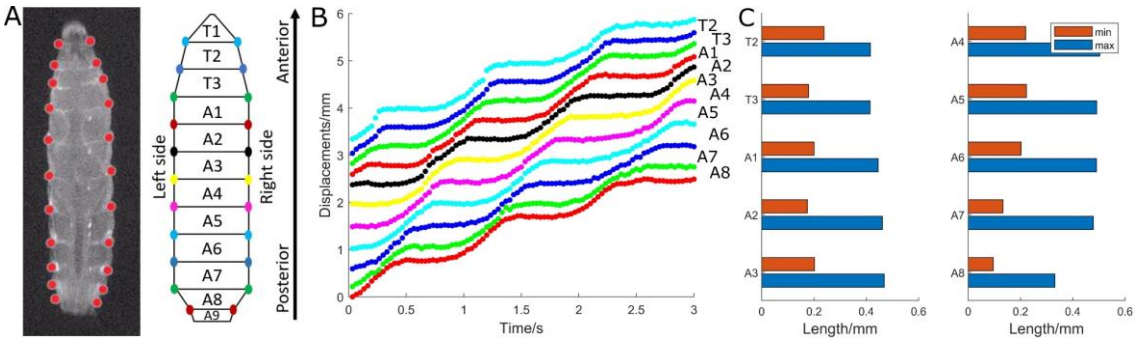

Figure 1. Characterization of forward crawling in third-instar larvae. (A) (left) Labelling of the segmental boundaries with fluorescence. The genotype is *tubP-Gal4, UAS-fondue::GFP*, (right) schematic of the thoracic and abdominal segments in the left panel. (B) Kymograph of segmental boundaries during forward crawling. Colouring corresponds to that in (A). (C) Minimum and maximum segment length during crawling.

Measurement of elastic and damping properties of larvae

Next, we analysed their physical properties. The stretchable body wall and hydrostatic skeleton of fruit fly larvae are typical components in soft-bodied organisms (Trueman, 1975). Previous studies have reported material properties of soft-bodied animals including the caterpillar *Manduca sexta* (Lin et al., 2009) and the earthworm *Lumbricus terrestris* (Quillin, 1998, 1999). Although a theoretical analysis of larval locomotion assumed that each segment is equivalent to a pair of a spring in parallel (an elastic component) and a damper (a viscous component) (Pehlevan et al., 2016; Ross et al., 2015), physical properties of *Drosophila* larvae have not been measured experimentally.

Viscoelastic properties of soft materials can be acquired by measuring the relationship between stress (force loaded in the material) and strain (deformation of the material) (Banks et al., 2011). To obtain viscoelastic properties of larvae, we conducted the stress relaxation test, one of the standard dynamic mechanical tests (Banks et al., 2011). In this test, we extended an anesthetized third-instar larva by 0.4 mm and recorded the stress in the larva decaying over time (Figure 2A). The result shows an exponential decay that is approaching

a non-zero plateau at a later time (Figure 2B). Among the general mechanical structure models of linear combinations of springs and dampers, we found that the Maxwell model and the Kelvin-Voigt model, which were used previously to model larval musculature (Pehlevan et al., 2016; Ross et al., 2015), could not fit the experimental curve well, since either exponential decay or residual elastic force is missing in these models (Supplementary Figure 2). In contrast, the SLS model, which combines the Maxwell model and a Hookean spring in parallel (Banks et al., 2011), fits the experimental results well. Thus, we fit this curve with the general SLS model (Figure 2B and 2C). According to the SLS model, we obtained the two spring constants and one damping coefficient from the data ($k1$ = 2.76$\pm$1.52 N/m, $k2$ = 2.88$\pm$1.42 N/m, c = 474$\pm$318 Nsec/m, from n=15 larvae, Figure 2C). Thus, we obtained a set of material parameters to describe the kinetic dynamics of fly larval body segments.

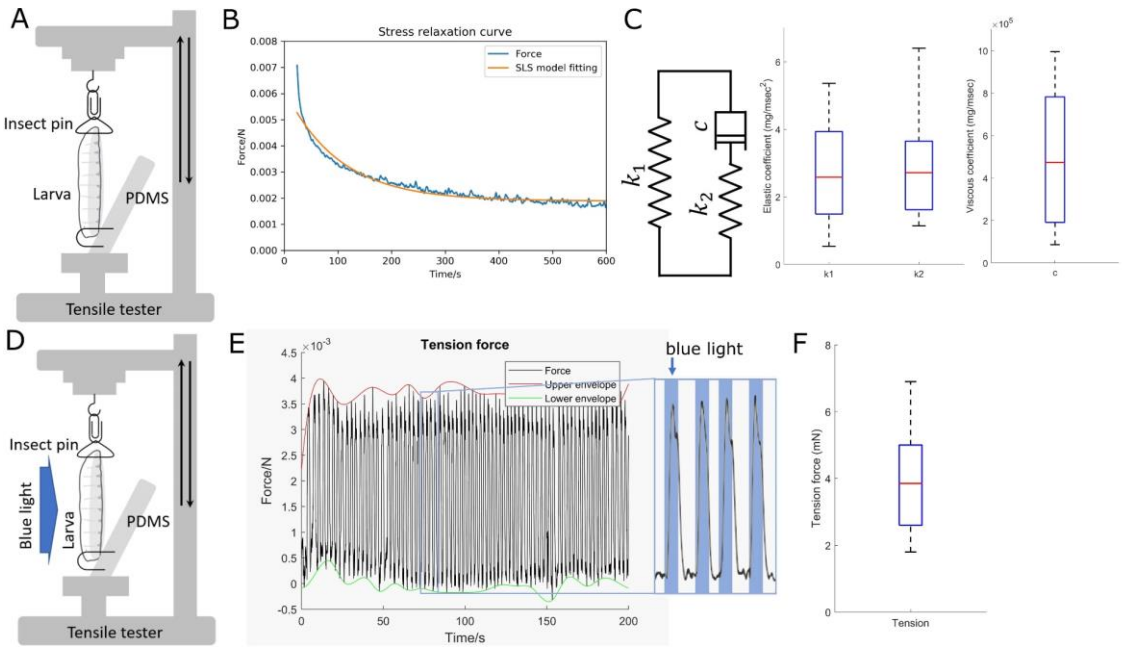

Figure 2. Physical measurement and experimental results for viscoelasticity and tension force. (A) Experimental setup for measurement of physical properties of larvae. (B) Example of the stress relaxation curve and fitting to the SLS model. (C) (Left) the SLS model, (right) the parameters obtained from the measurement of 15 larvae. (D) Experimental setup

for the tension measurement via optogenetics. (E) Traces of force upon optogenetic activation. Blue light was applied for 2 seconds (shown blue shades in the right panel) with 2 seconds interval. Red and green envelopes show the local maximum and minimum forces, respectively (the size of the time window for calculating the local extremums is 6.5 sec). (F) Contraction forces obtained from 18 larvae.

Measurement of contraction force of larvae with optogenetics

We next measured the muscular force of larvae that is acting on segments, and the actuator origin of larval locomotion. While one previous study measured muscle force in semi-intact fly larvae (Paterson et al., 2010), muscle contraction force in intact larvae remains unknown. To reliably activate motor neurons in intact larvae for force measurement, we applied optogenetics (Kohsaka et al., 2014). We expressed a light-sensitive cation channel protein Channelrhodopsin2 in motor neurons and illuminated each larva with blue light (455 nm, 5.7 nW/mm^2) to activate the motor neurons in the intact larva (Figure 2D). We measured the contraction force elicited by the optogenetic activation (3.99 ± 1.51 mN, n=18 larvae, Figure 2E, F). In sum, we succeeded in obtaining both passive (the spring constant and damping coefficient) and actuating (the contraction force) properties of segments.

A novel neuromechanical model based on physical measurements

Based on the physical measurements described above and biological evidence obtained by previous studies, we established a neuromechanical model. In this model, segmental boundaries are regarded as masses, which are pulled and pushed by segmental muscles and drag on the surface with friction (Figure 3A). Based on the stress relaxation test described above, we adapted the SLS model for the physical properties within segments (Figure 3A). The muscles are modelled as tension actuators.

Regarding neural circuits, recent connectomics studies have identified several key interneurons in the motor circuits in fly larvae (Clark et al., 2018; Kohsaka et al., 2017). From

among the interneurons, we focused on the A27h and GDL interneurons, since they are involved in the forward propagation of neural activity (Fushiki et al., 2016). A27h and GDL are segmentally repeated interneurons. The A27h premotor neuron is rhythmically activated during forward but not backward locomotion (Clark et al., 2018; Fushiki et al., 2016). A27h activates motor neurons in the same segment and GDL in the next anterior segment, while GDL inhibits A27h in the same segment (Fushiki et al., 2016). Thus, A27h and GDL form an intersegmental feedforward chain and may contribute to signal propagation from the posterior to anterior segments. Based on the A27h-GDL connectivity, we established a circuit model of a linear chain of excitatory and inhibitory neurons (Figure 3B). In the A27h-GDL circuit model, we introduced a rebound property of excitatory neurons that enables the excitatory neurons to be activated just after the termination of inhibitory inputs from GDL onto A27h neurons to convey the propagation. This A27h-GDL model can exhibit propagation of activity from the posterior to anterior segments (Supplementary Figure 3), which implies that the A27h-GDL motif can work as a circuit component in the integrated neuromechanical model. To complete the neuromechanical model, we added a sensory feedback module and efferent control for motor output (Figure 3C). After tuning parameters in the circuit model, while keeping physical parameters as measured, we found that computer simulation shows that our neuromechanical model can generate crawling behaviour and segmental dynamics (Figure 4B) that replicates the kinematic measurement results (Figure 4B, middle).

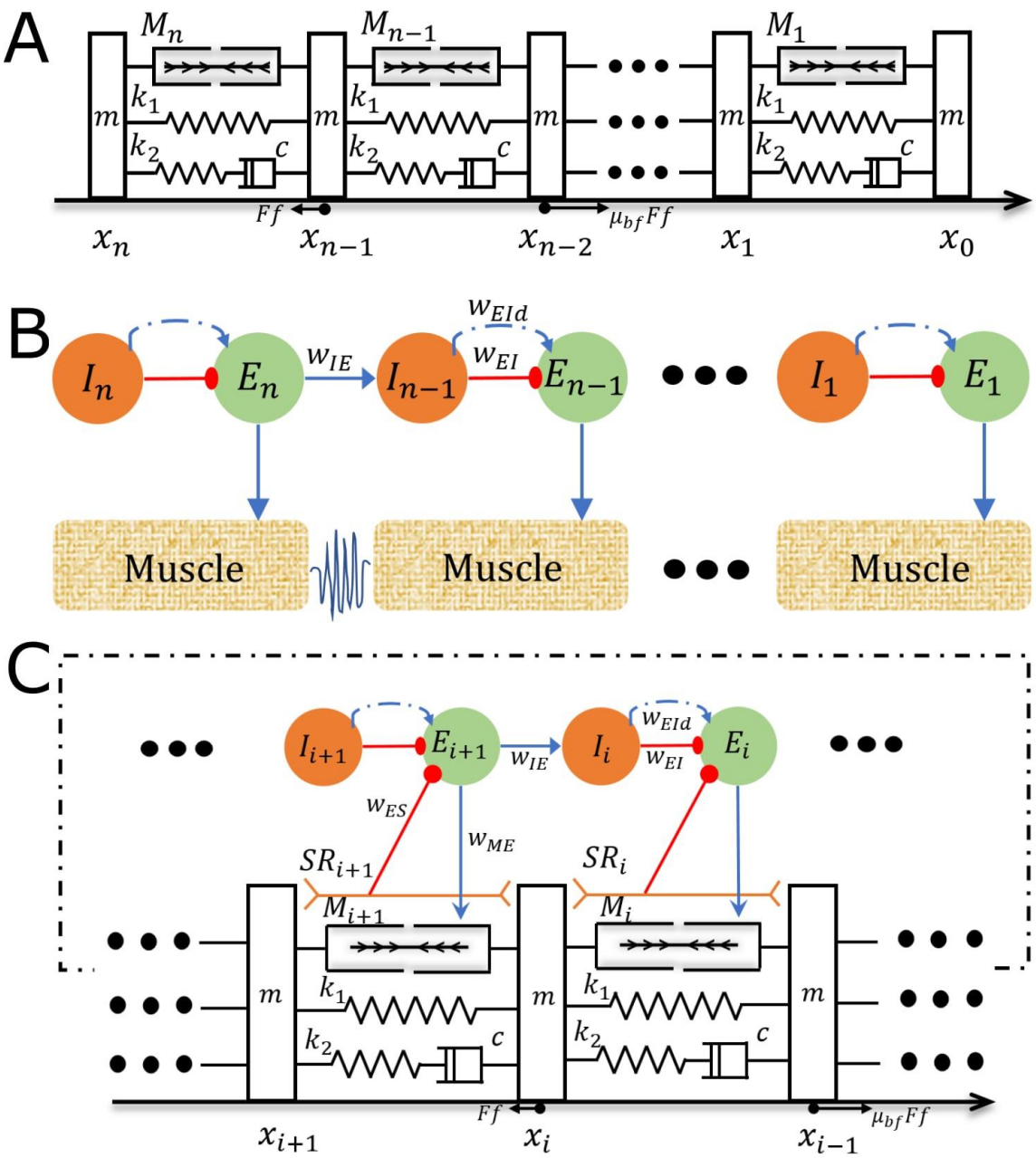

Figure 3. Framework for the neuromechanical modelling. (A) Mechanical framework for *Drosophila* larvae. The mechanical structure consists of repetitive segments, with mass block m, tension actuator M_i and SLS module (with k_1, k_2, c) in parallel connection. x_i denotes the position of the segment boundary. Asymmetric friction f (Ff for forward friction, $\mu_{bf}Ff$ for

backward friction) happens during locomotion. (B) Neural chain for feedforward control. Based on the GDL-A27h circuit, GDL is modelled as an inhibitory population I_i, while A27h is modelled as an excitatory population E_i to activate muscle groups. Segmental muscles are mechanically coupled along the longitudinal axis. (C) The integration of mechanical model and neural circuits including the neural chain, efferent signals and sensory feedback. The muscular tension is generated by muscles M_i. Sensory feedback SR_i is driven by the change in the segmental length.

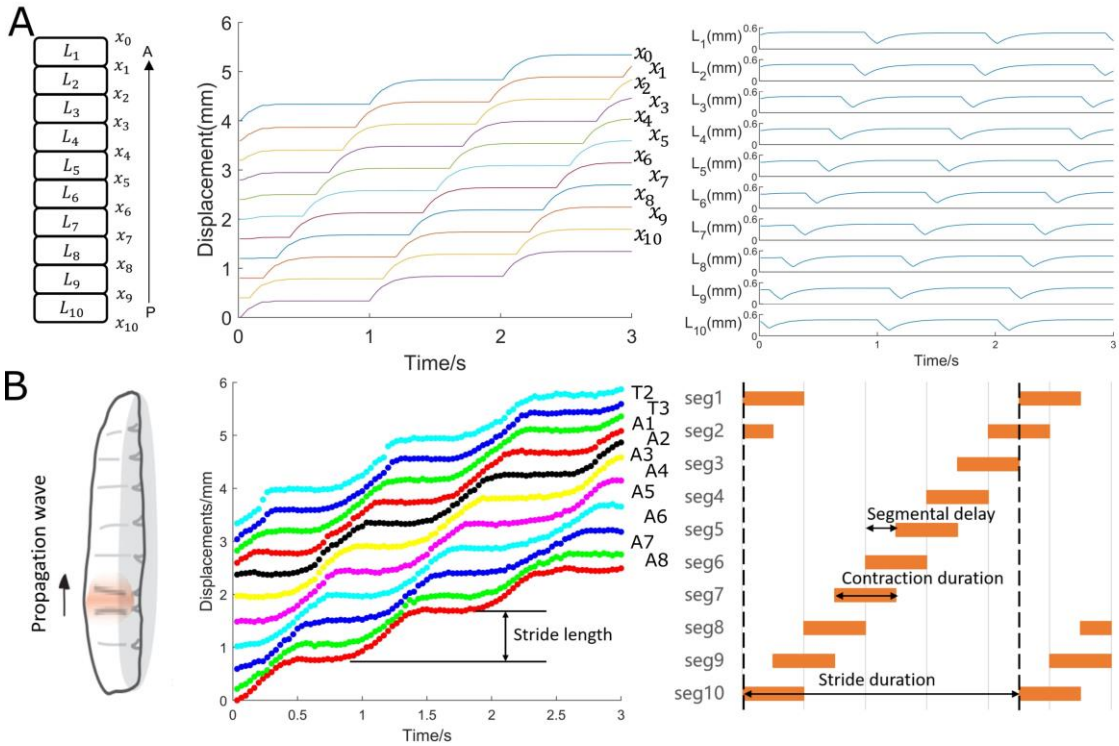

Figure 4. Simulation responses based on the neuromechanical model. (A) (Left) sketch of the mechanical model for *Drosophila* larvae, (middle) kymograph of segmental boundaries in the neuromechanical simulation, (right) traces of segmental lengths in the neuromechanical simulation. (B) (Left) schematic of third-instar larva, (middle) kymograph of segmental boundaries during forward crawling measured experimentally, the same panel as that in Figure 1B, (right) the definition of spatiotemporal indexes for analysis of forward

locomotion of *Drosophila* larvae. Orange bars mark the duration during which segmental muscles are contracted.

Kinematic analyses for larval crawling

Using the neuromechanical model, which follows the soft body material properties of larvae and mimics kinematic dynamics of free-moving larvae, we examined the dependency of larval crawling on each of the model parameters. To analyse the mechanisms in the change of crawling properties, we measured stride frequency and stride length (Figure 4B). The stride frequency (calculated by the inverse of stride duration) shows how often crawling steps occur, and the stride length notes how far the larvae move in a single stride. Accordingly, the crawling speed can be decomposed to the product of the stride frequency and stride length. To further analyse the segmental kinematics, we also calculated contraction duration and segmental delay (Figure 4B). Using these values to describe locomotion properties, we examined the following five potential factors that may affect motor patterns: 1) viscoelasticity of the body; 2) body-substrate interaction; 3) the feedforward neural chain; 4) motor output; and 5) proprioceptive feedback.

Viscoelasticity

We analysed the effect of viscoelasticity in the mechanical structure (Figure 5A-F). First, we examined the contribution of elasticity and viscosity. In the SLS model, the viscoelasticity is embodied in the spring constants k_1, k_2 and damping coefficient c. The physical measurements found the data range for k_1, k_2 and c are 2.76$\pm$1.52 N/m, 2.88$\pm$1.42 N/m, and 474 ± 318 N$\cdot$sec/m, respectively (Figure 2C). The values obtained by physical measurements are marked as stars in the following simulations (Figures 5 – 8). When the viscosity (damping coefficient c) changed, the locomotion properties, including speed, stride frequency, stride length, and segmental dynamics, are less affected (Figure 5B, C), suggesting kinematics in crawling does not depend on the viscosity. On the other hand, the

locomotion speed increases when the elasticity (spring coefficients k_1 and k_2) decreases (Figure 5E, F). To analyze this phenomenon, we examined the stride frequency and stride length and found that this increase in the speed at low k_1 or $k_2$value is due to the long stride length, whereas the stride frequency is less affected (Figure 5F). Consequently, the elastic property of the larval body seems to play a more important role in the locomotion, compared with the viscosity. Furthermore, the simulation shows that the speed of crawling can be increased by decreasing elasticity (Figure 5E). By replacing body wall material with materials of lower elasticity, larvae can crawl faster. Accordingly, we conclude that the elasticity of the body is one of the key factors in regulating the speed of crawling in intact larvae. In the following simulation, we set the viscoelastic values to the measured values ($k1$=3 N/m, $k2$=3 N/m, c=475 N sec/m).

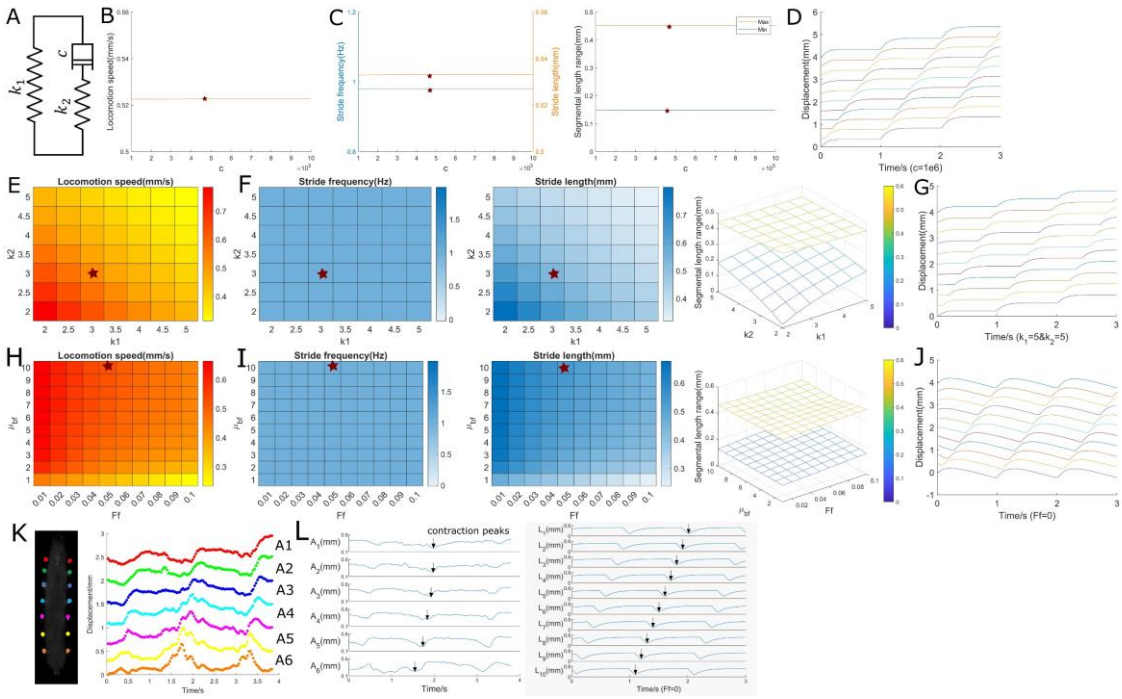

Figure 5. Kinematic analysis of the effects of viscoelasticity and friction. (A) Sketch of the SLS model. (B) Model responses of locomotion speed in the perturbation of viscous parameters. (C) Model response of stride frequency (left panel, blue curve), stride length (left,

orange curve), segmental length range (right panel, upper orange curve for maximum segmental length, and bottom blue curve for minimal segmental length) in the perturbation of viscous parameters. (D) Plot of segment displacement with a large c value. (E) Responses of locomotion speed in the perturbation of elastic parameters. (F) Responses of stride frequency (left), stride length (middle), and segmental dynamics (right, upper orange surface for maximum segmental length, and bottom blue surface for minimal segmental length) in the perturbation of elastic parameters. (G) Trace of segment displacement with high elastic parameters. (H) Responses of locomotion speed in the perturbation of friction conditions. (I) Responses of stride frequency (left), stride length (middle) and segmental dynamics (right, upper blue surface for maximum segmental length, and bottom orange surface for minimal segmental length) in the perturbation of friction conditions. (J) Plot of segment displacement without friction force F_f. (K) The snapshot of larval crawling while floating in the high concentration sugar solution (left), and its segmental kymograph over time (right). (L) Segmental length changes of the experimental (left) and simulation (right) results, corresponding to the Figure 5K and 5J, respectively. Arrows indicate the propagation of muscle contraction in forward crawling. (All the stars in B-F, H and I refer to the default configurations of parameters in the neuromechanical model.)

Body-substrate interaction

Next, we analysed the effect of friction. Friction force is difficult to measure due to its dynamic and non-linear nature. In our simulation, the default basic friction force F_f was set to 0.05 mN based on a previous experimental result for a glass fibre mimicking small nematodes (0.05 mN) (Wallace, 1969). A major origin of the friction between the larval body and the ground surface is the denticle belts, which are aligned at the bottom of the body and oriented anteriorly (Repiso et al., 2010). Because of this asymmetric nature of the denticle belts, friction force on a segment is higher in backward motion than in forward motion. So, we modelled friction force in the forward direction as F_f and that in the backward direction as

$\mu_{bf}\ F_f$ where μ_{bf} > 1 (Figure 5F) (Paoletti and Mahadevan, 2014). When we perturbed the forward friction F_f and asymmetric forward-backward friction ratio μ_{bf}, we found that the speed of locomotion is higher at weaker friction forces and larger asymmetric ratio (Figure 5H left). To analyze this phenomenon, we decomposed the speed into the stride frequency and stride length. Whereas the stride frequency is not affected in this range (Figure 5I), which is consistent with the observation in a previous simulation (Pehlevan et al., 2016), the stride length is larger at low Ff and high μ_{bf} (Figure 5H right). This would be because a larger friction force dissipates more kinematic energy and induces shorter segmental translocations (Figure 5F, (Ross et al., 2015)). A larger asymmetric coefficient μ_{bf} allows larger stride length, which would help in the avoidance of slippage to stabilize forward crawling (Figure 5I). When the friction is removed, the model larvae show slippage and cannot move forward while showing propagation waves (Figure 5J), suggesting friction contributes to the avoidance of slippage but not to the propagation per se. To test this simulation observation, we measured crawling behaviour in a low-friction environment. We used a high concentration sugar solution (66% w/w sucrose) and floated third-instar larvae in it. In this low-friction environment, the larval body can also exhibit the propagation of segmental contraction, while remaining almost in the original position (Figure 5K), as in the simulation response (Figure 5J). The speed of propagation in floating larvae (10.3 segments / sec (n = 2)) is comparable to that in the simulation with zero friction (9.9 segments / sec (n = 3)). In summary, analyses of friction force imply two points: 1) In a high friction and low forward-backward asymmetric condition, larvae crawl slower; 2) In a low friction condition, propagation of segmental contraction can be generated, even though the larvae are hardly to move forward.

Feedforward neural chain

The neural model we developed is a CPG model based on the GDL-A27h neural chain (Fushiki et al., 2016). This circuit contains three groups of parameters: synaptic weights,

relaxation constants, and activation thresholds. We perturbed these values and analysed their effects on locomotion.

This circuit consists of three synaptic weights, w_{IE} , w_{EI} and w_{EId} (Figure 6A left). Excitatory weight w_{IE} is a synaptic weight from excitatory neurons to inhibitory neurons in the next anterior segment, and has a positive value to activate postsynaptic neurons. Inhibitory weight w_{EI} is a weight from inhibitory neurons to excitatory neurons in the same segment, and has a negative value to suppress postsynaptic neurons. Considering a previously suggested phenomenon that the declining of GDL activity releases the target A27h from its inhibition (Fushiki et al., 2016), we introduced the rebound weight w_{EId} to denote a coefficient to time-derivative of presynaptic neurons. The product of w_{EId} and the time-derivative of presynaptic neuron activity is input to postsynaptic neurons in our model. By setting w_{EId} to be negative, the rebound property of inhibitory neurons was modelled. The activity of excitatory and inhibitory units (E and I) with default parameter configuration is depicted in Figure 6A right. When we changed w_{EI}, the speed of locomotion was less affected (Figures 6B). On the other hand, when we changed w_{IE} and w_{EId}, the speed of locomotion was changed (Figures 6D, F). Regarding the excitatory synapses, smaller w_{IE} leads to faster crawling. This is because a smaller excitatory weight w_{IE} limits the activation duration of the Inhibitory unit (Supplementary Figure 4B), shortening the intersegmental delay, which gives rise to the larger stride frequency, although with a slight decrease in segmental dynamics (Figure 6D). Similarly, while the inhibitory weight w_{EI} seems to play less important roles in crawling dynamics, rebound weight w_{EId} has a critical role in the speed of locomotion (Figure 6D). Smaller absolute values of w_{EId} gives faster crawling speed due to higher stride frequency (Figure 6E) by shortening the activation duration of the excitatory unit (Supplementary Figure 4B). Along the feedforward chain, w_{IE} and w_{EId} have similar functions, working for the target activation and following rebound respectively (Figure 6F). The effects of w_{EId} are like that of w_{IE}, in that their larger weights result in longer contraction duration and increased stride duration, which decreases the speed of locomotion.

We next analysed the effect of relaxation constants and activation thresholds in the neural circuit model. Relaxation constants determine the rate of rising and falling in the neural activities (Supplementary Figure 4C). We examined relaxation time constants of excitatory neurons τ_E and inhibitory neurons τ_I. We found that either large τ_E or small τ_I gives faster crawling (Figure 6H). The stride frequency is not affected by τ_E (Figure 6I) whereas stride length increases when τ_E is larger (Figure 6I), due to the long period of muscle contraction inducing larger segmental length change (Figure 6I). By this mechanism, the speed of locomotion is faster under high τ_E. On the other hand, the effect of small τ_I arises from a different mechanism: in the small τ_I condition, stride frequency increases (Figure 6I) because the rising and falling period in I units is small, and this in turn increases the speed of locomotion when τ_I is small. To summarise: the relaxation constants of excitatory and inhibitory units affect the speed of locomotion by distinct mechanisms. As for the activation threshold, we examined a threshold of excitatory neurons θ_E and that of inhibitory neurons θ_I. The thresholds define the minimal input for neurons to be activated, affecting their burst duration (Supplementary Figure 4D). In larger θ_I, the speed of locomotion becomes faster (Figure 6J). Under these conditions, the stride length is less changed but the stride frequency becomes larger (Figure 6K), owing to the function of I units as intersegmental delays. Consequently, through perturbation of parameters in the neural circuit model, we found there exist distinct mechanisms to change the speed of crawling.

So far, we analysed synaptic weights, relaxation constants and activation thresholds in the A27h-GDL model and found the dependency of locomotion on these parameters. To test whether these tendencies are general, we analysed another neural circuit model described in Pehlevan et al (Pehlevan et al., 2016) with our mechanical model based on the SLS model with measured physical parameters. The model described by Pehlevan can also produce sustainable segmental translocations; corresponding results are shown in Supplementary Figure 4E. Both neural stimuli can sustain a periodic propagation wave based on the physical structure (Figure 3 and Supplementary Figure 4E). Based on their default neural connection

and synaptic weights, we perturbed the two main groups of parameters, time relaxation constants and activation thresholds, and found a similar dependency on them in crawling frequency and speed (Supplementary Figure 4F, G). Consequently, the tendency of dependence on these parameters should be a general property. In addition, by controlling these circuit parameters, the speed of crawling can be regulated.

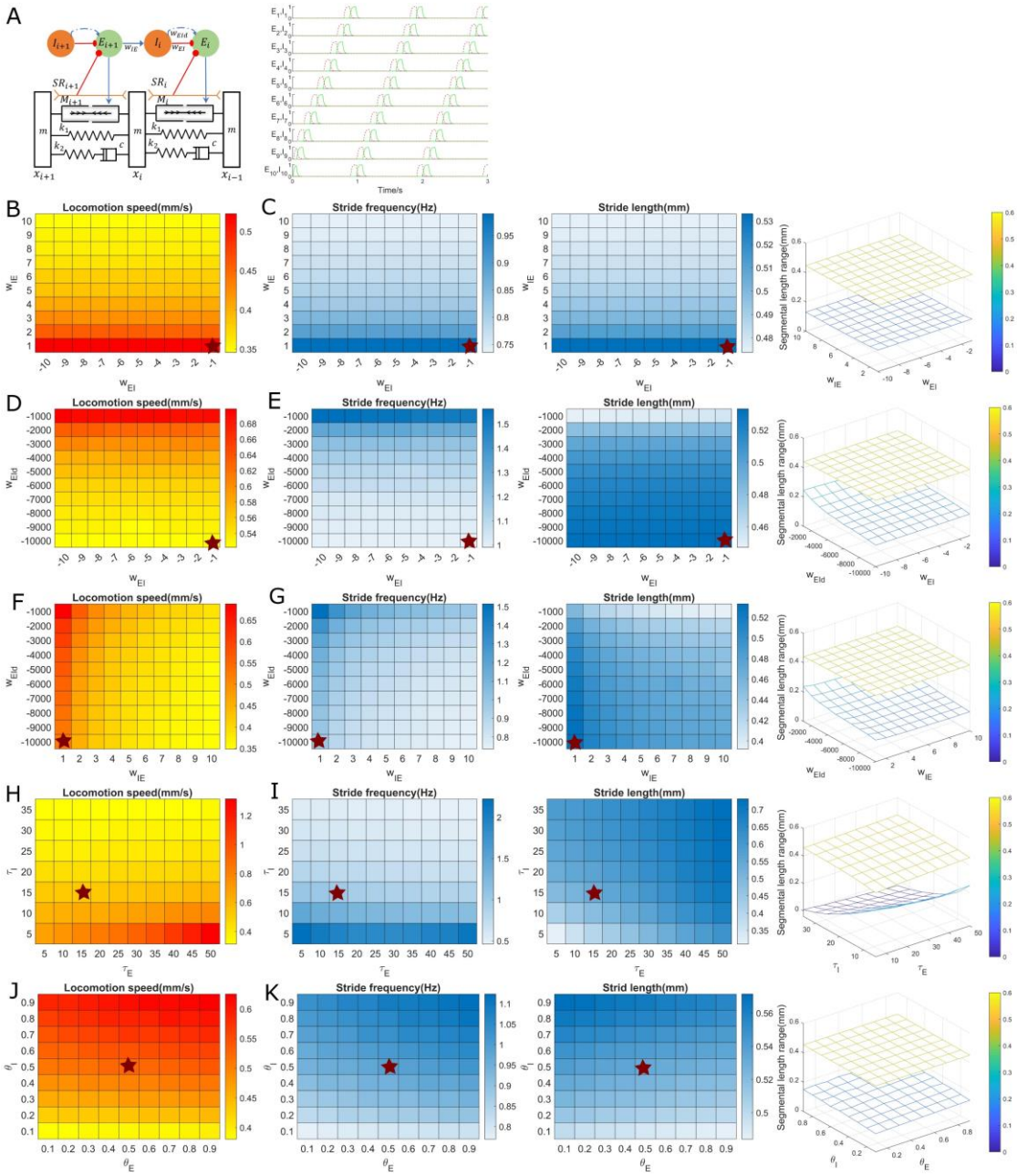

Figure 6. Kinematic analysis of the effect of neural circuits. (A) Sketch of the neural configuration in the neuromechanical model (left), and traces of activity in excitatory and inhibitory neural units (right). (B-G) Responses in the perturbation of neuronal parameters. Locomotion speed (B, D and F), stride frequency (left in C, E and G), stride length (middle in C, E and G) and segmental length change (right in C, E and G), in a range of connection weight pairs, $w_{EI} - w_{IE}$ (B and C), $w_{EI} - w_{EId}$ (D and E), $w_{IE} - w_{EId}$ (F and G). (H-I)

Responses in the perturbations of time relaxation constants of E-I populations. (J-K) Responses in the perturbation of activation threshold of the E-I populations. (All the stars in B-K refer to the default configurations of parameters in the neuromechanical model.)

Motor output

We next analysed the effects of muscular contraction properties on crawling (Figure 7). We described muscle using three factors: maximum tension $F_{M_{max}}$, time relaxation constant τ_M and threshold for activation θ_M.

We changed the maximum tension force (Figure 7B-D) and found that larger tension increases the locomotion speed (Figure 7B). This is because a longer stride length can be achieved with a stronger tension force, while the stride frequency is less affected. When τ_M is larger, the speed of locomotion becomes slower (Figure 7E). This may be because a slower uprising of muscle force leads to shorter stride length (Figure 7F). The third factor is the activation threshold θ_M. When θ_M is large, the speed becomes slower (Figure 7H), which may be due to a smaller amplitude in contraction force (Figure 7J) and stride length (Figure 7I), while its frequency does not change significantly since it follows the wave propagation along the feedforward chain.

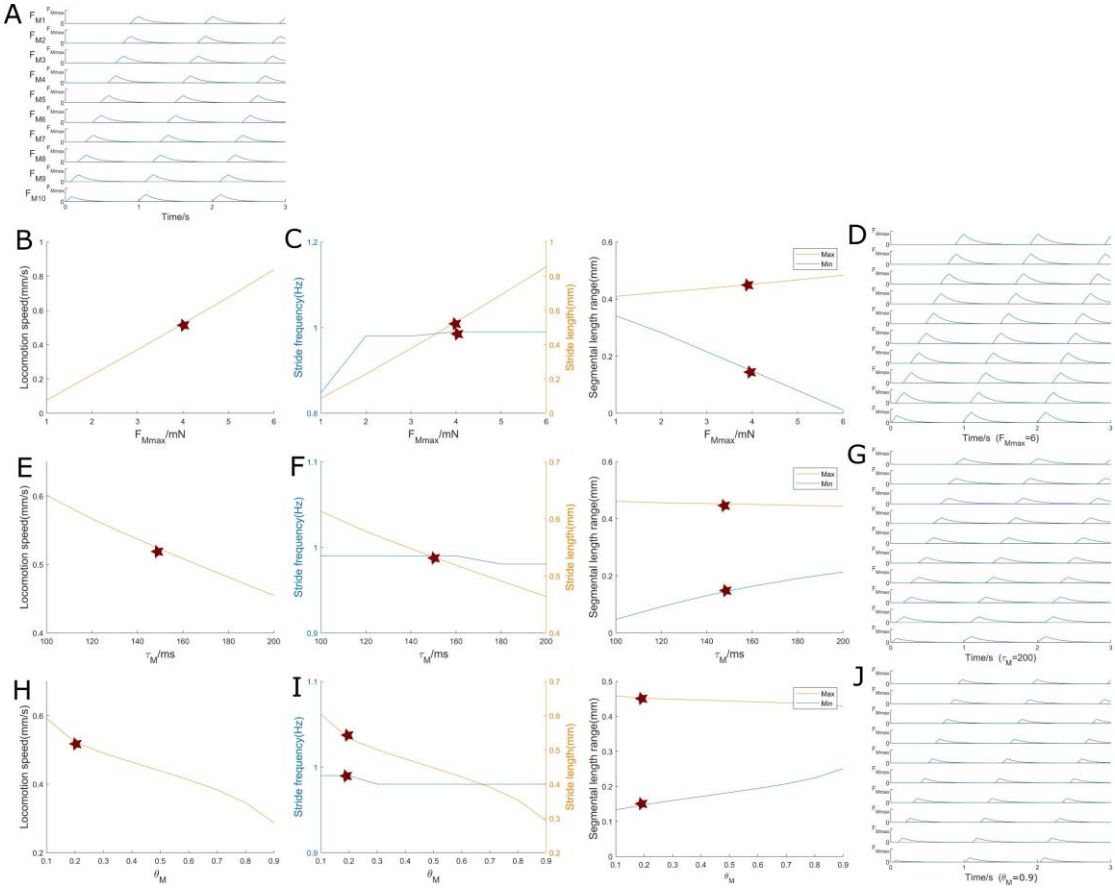

Figure 7. Kinematic analysis of the effect of efferent control. (A) Traces of muscular forces in the default configuration of the parameters. (B-C) Responses of speed (B), stride frequency (blue curve in C left), stride length (orange curve in C left), and maximum (blue curve in C right) and minimum length (orange curve in C right) of segments in the perturbations of tension force. (D) Traces of tension forces with a large amplitude in tension force. (E-F) Responses of speed (E), stride frequency (blue curve in F left), stride length (orange curve in F left), and maximum (blue curve in F right) and minimum length (orange curve in F right) of segments in the perturbations of time relaxation constant of muscles. (G) Traces of tension forces with a large time relaxation constant. (H-I) Responses of speed (H), stride frequency (blue curve in I left), stride length (orange curve in I left), and maximum (blue curve in I right) and minimum length (orange curve in I right) of segments in the perturbations of the threshold of muscle activation. (J) Traces of tension forces with a large amplitude in

the threshold of muscle activation. (All the stars in B, C, E, F, H and I refer to the default configurations of parameters in the neuromechanical model.)

Proprioceptive feedback

In our neuromechanical model, we implemented proprioceptors to sense the length of segments and send inhibitory signals to excitatory components in the circuits (Figure 8A). There are two parameters on the sensory neurons: threshold for length sensing θ_S, which is a maximum segment length to activate proprioceptors, and synaptic weight W_{ES}, which is a negative value reflecting the inhibitory role of sensory feedback. The sensory feedback signal becomes stronger when the sensing threshold θ_S is higher and the synaptic weight is larger. As Figure 8 shows, the speed of locomotion becomes slow without proprioceptive feedback (e.g. W_{ES} = 0) or when the sensitivity of the proprioceptive neuron is very low (Figure 8B, when θ_S is smaller than 0.4). Meanwhile, the locomotion frequency becomes larger with increasing proprioceptive feedback (Fig 8C), which is consistent with the descriptions in previous works (Hughes and Thomas, 2007; Pehlevan et al., 2016).

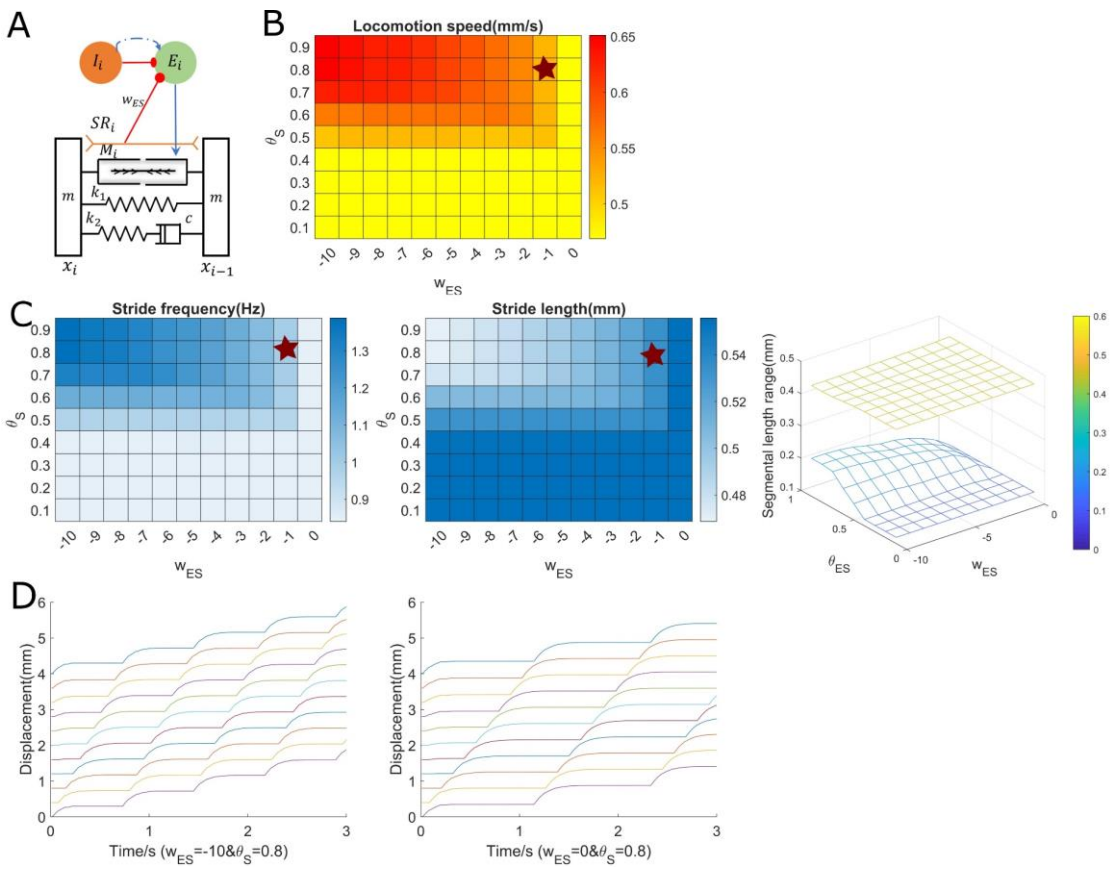

Figure 8. Kinematic analysis of the effect of proprioceptive feedback from sensory receptor to the feedforward chain. (A) Sketch of the proprioceptive sensory feedback components. (B-C) Responses of speed (B), stride frequency (C left), stride length (C middle), and segmental length change (C right) in the perturbation of sensory feedback. (D) Traces of segment displacement with large (left) and small (right) sensory feedback. (All the stars in B and C refer to the default configurations of parameter in the neuromechanical model.)

Determinants of larval crawling speed

From the systematic analysis described above, we obtained the dependency of every parameter in the model on the locomotion pattern. Figure 9 summarises the relation map on the crawling speed. We tested parameters in the following components: body viscoelasticity, motor outputs, body-substrate interaction (friction forces), feedforward neural chain, and

proprioceptive feedback. Larval locomotion speed depends on most of these parameters except for viscosity. The relation map indicates that these components can be classified as spatial and temporal factors. Viscoelasticity, muscular forces, and body-substrate interaction affect the crawling speed through the stride length, which indicates these parameters modulate spatial factors in the crawling speed. On the other hand, the neural circuits control the crawling speed mainly through the stride frequency. This analysis implies that tuning each of these spatial and temporal aspects underlies the determination of the crawling speed. Consequently, while the neural circuits mainly contribute to temporal aspects in the crawling speed, the physical components also have significant roles in crawling speed through spatial aspects.

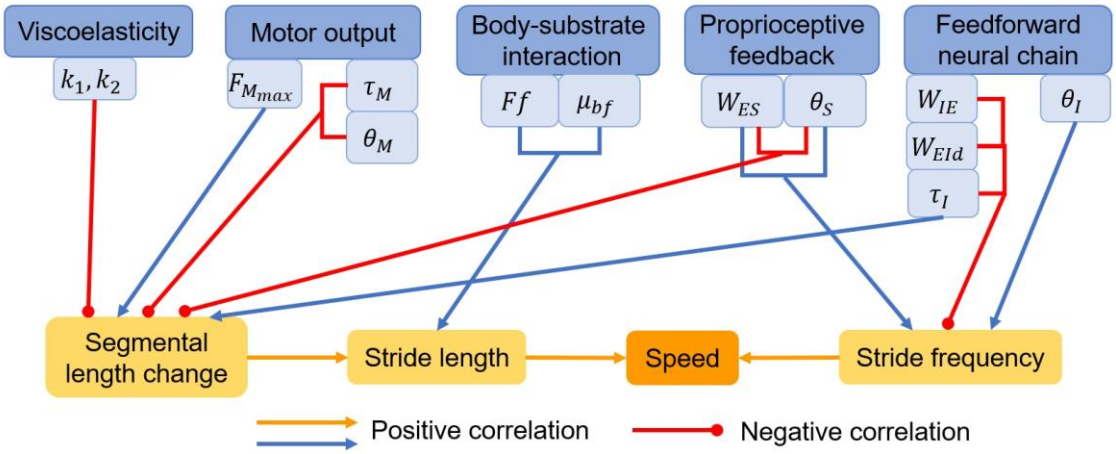

Figure 9. A correlation map of neuromechanical model parameters and locomotion properties. Arrows show positive correlation and arrows with round tips denote negative correlation.

Discussion

In this work, physical experiments on *Drosophila* third-instar larvae were conducted to obtain mechanical values, including viscoelasticity and tension force (Figures 1 and 2). These results suggest that the larval body should be modelled as a chain of mass and SLS modules (Figure 3), which is distinct from the previous modelling for larvae (Paoletti and Mahadevan, 2014; Pehlevan et al., 2016; Ross et al., 2015). Meanwhile, a neuromechanical model was proposed based on physical measurements and a biological finding, the GDL-A27h neural chain (Fushiki et al., 2016). The mechanical connection and sensory feedback are integrated via muscle control and sensory feedback. This model would be a useful framework to investigate the neuromechanical system of fly larvae as a soft-bodied animal, and it can produce the sustained forward strides from posterior to anterior terminal, consistent with the experimental results (Figure 4) (Berrigan and Pepin, 1995; Heckscher et al., 2012).

Speed of animal locomotion is one of the critical factors for survival. Based on our neuromechanical model, we examined the effect of various parameters on the speed of locomotion and analysed the mechanisms behind them. Except viscosity, most of the physical parameters (elasticity, friction, and muscle force) and neural ones (activity dynamics of excitatory and inhibitory units, motor outputs, sensory feedback) are involved in the speed of locomotion. Interestingly, we found that a change in most of the parameters produced a boost in the speed of locomotion in the simulation, as shown in Figure 9. The submaximal nature of the crawling speed implies that the value of intact larval speed resides in a continuum parameter space of the neuromechanical system. Considering the crawling speed of *Drosophila* larvae is almost uniform in a fixed condition, the observation of the submaximal nature implies the existence of additional factors to regulate the speed of locomotion. These factors may include physiological components, especially energy consumption. By changing parameters, such as muscle contraction force or sensory feedback signal, some cost should be paid, for example the supply of ATP to muscles or the expression of more proteins at the presynaptic terminal of sensory neurons. By analysing physiological economy in the

neuromechanical system as a whole, we will gain a deeper insight into the tuning of kinematic parameters for animal locomotion.

With respect to future prospects of this study, it diverges in two directions. The first is to integrate other neural circuit modules into this model, e.g. modules for bilateral coordination (Heckscher et al., 2015), turning (Clark et al., 2018; Kohsaka et al., 2017) and sensory-guidance (Garrity et al., 2010; Louis et al., 2008; Luo et al., 2010; Takagi et al., 2017), to better replicate the locomotion characteristics of the *Drosophila* larva. Secondly, we anticipate that the notions in the neuromechanical system can serve biomimetics. In recent decades, more and more soft robots, endowed with new capabilities relative to the traditional hard ones, have been designed to exhibit complex movements (Aguilar et al., 2016; Corucci et al., 2018; Kim et al., 2013; Trivedi et al., 2008). Taking *Drosophila* larvae as a prototype, the bionic structure can be established with high dexterity to explore the unstructured environments. Meanwhile, the response of the neuromechanical model can be utilized to control the locomotion of soft larval robots to the greatest extent, to mimic locomotion properties from the biomimetic perspective.

Materials and Methods

Viscoelasticity measurement

The genotype we used for viscoelasticity measurement was a wild type Canton S. The third-instar larvae in the feeding stage were washed with distilled water and dried with paper. Each larva was placed into an enclosed petri dish filled with evaporated diethyl ether. The larvae remain immobile for several hours after being exposed to diethyl ether for around four minutes (Kakanj et al., 2020). When the larvae were immobile, insect pins were inserted into the head and tail. The pin in the head was bent to form a loop to hook to a paper clip that was hung on the hook of the tensile sensing machine, while the pin in the tail was used to fix the body on the PDMS (Polydimethylsiloxane) silicone block, held by the tong on the

SHIMADZU EZ-S platform with a 5 N load cell. The experimental equipment is shown as Figure 2A. The larval body was kept in the vertical axis for measurement. The baseline of force was calibrated by values measured before the application of external elongational force. All the experimental procedures were performed at room temperature.

During the stress relaxation tests, we applied a constant strain of 0.4 mm, 10% of the body length (4 mm), to the larvae. The time-dependent stress decreased until the plateau was reached after a while, as shown in Figure 2B. To fit the stress relaxation curve to mechanical analogues, we adapted the Maxwell model, the Kelvin-Voigt model and the standard linear solid (SLS) model. These models give the relationship between joint force F and displacement ΔL. Detailed functions are described as follows:

$$\frac{F}{c} + \frac{1}{k}\frac{dF}{dt} = \frac{d\Delta L}{dt} \qquad \text{Maxwell model}$$

$$F = k\Delta L + c\frac{d\Delta L}{dt} \qquad \text{Kelvin-Voigt model}$$

$$F + \frac{c}{k_2}\frac{dF}{dt} = k_1\left(\Delta L + c\frac{k_1+k_2}{k_1k_2}\frac{d\Delta L}{dt}\right) \qquad \text{SLS model}$$

where k and c are the elastic and damping constants, respectively. The total displacement of 0.4 mm was realised by pulling the larval body with a velocity of 1 mm/min. During the stress relaxation experiments, this elongation time (24 sec) is much shorter than that for relaxation (576 sec), and thus the displacement is regarded as the step function $L(t) = L_0H(t-t_0)$ and initial force is $F(0) = 0N$, where $L_0 = 0.4\,mm$ and $H(t)$ is the Heaviside step function. In this case, the corresponding stress relaxation functions in these models are described as follows:

$$F = ke^{-\frac{k}{c}(t-t_0)}L_0H(t-t_0) \qquad \text{Maxwell model}$$

$$F = kL_0H(t-t_0) + cL_0\delta(t-t_0) \qquad \text{Kelvin-Voigt model}$$

$$F(t) = \left[k_1 + k_2e^{-\frac{k_2(t-t_0)}{c}}\right]L_0H(t-t_0) \qquad \text{SLS model}$$

where $t_0 \geq 0$. By fitting these curves to the stress-relaxation measurement data, we obtained the spring constants and damping coefficients. We used Python 3.7 for the curve fitting.

Contraction force measurement with optogenetics

For optogenetic activation of motor neurons, we used the *OK6-GAL4, UAS-ChR2* line (Kohsaka et al., 2014). The early third-instar larvae were selected and put into ATR (all-trans-retinal) containing yeast paste, the concentration of which was 1 mM. These larvae were reared at 25 °C in the dark for one day (Matsunaga et al., 2013). Afterwards, the third-instar larvae were prepared for measurement of tension force as described above (Viscoelasticity measurement section). Blue LED light (455 nm, 5.7 nW/mm^2, M455L3, ThorLab) was used to stimulate ChR2 expressed in motor neurons, which leads to the contraction of the larval body. In each stimulation, the blue light was applied for two seconds followed by a no-illumination interval of two seconds, and the force induced was monitored. Eighteen larvae were used in the measurement and each measurement took two to five minutes. The optogenetically induced forces were measured by the differences between forces during illumination and no illumination (Figure 2D).

Larval crawling in a low-friction environment

We used a high concentration sugar solution (66% w/w sucrose) and floated third-instar larvae in it. The genotype we used was *R70C01-Gal4, UAS-CD4::GFP*, which allowed us to mark the abdominal segmental boundary from A1 to A7. The locomotion was recorded via SZX16 fluorescent microscope (Olympus, Japan) with 1.25x object lens at 30 frames/sec, and its trajectory was measured by Fiji (Schindelin et al., 2012).

Modelling

Body-substrate mechanics and modelling

As we mentioned before, the larval crawling stride consists of a piston phase and a wave phase (Heckscher et al., 2012). The piston phase constrains the larval body length to be almost constant, while the wave phase generates the propagation wave repetitively. To make it simple, we modelled the whole body of larvae as a chain of eleven segments.

We assumed that the model framework possesses the constant length and its segments are entirely repetitive based on the observation in Figure 1C. Then the body is modelled as a chain of the SLS units in series (Figure 3A). Muscle groups are modelled as the tension actuator to accept efferent control from the neural circuit (Figure 3C). The tension F_M is the contraction force to counteract the effect of body viscoelasticity and friction. Viscoelasticity was described as a combination of springs and damper. The mechanics are described based on the Newton's second law as follows.

$$\begin{cases} m\ddot{x}_0 = m\ddot{x}_n = F_n - F_1 + F_{M_n} - F_{M_1} - f_0 \\ m\ddot{x}_i = F_i - F_{i+1} + F_{M_i} - F_{M_{i+1}} - f_i \quad i = 1, \dots, n-1 \\ x_0 = x_n + nL \end{cases}$$

$$F_i + \frac{c}{k_2}\frac{dF_i}{dt} = k_1\left(x_{i-1} - x_i - L + c\frac{k_1+k_2}{k_1k_2}\left(\frac{dx_{i-1}}{dt} - \frac{dx_i}{dt}\right)\right)$$

$$\tau_M \dot{F}_{M_i} = -F_{M_i} + F_{M_{max}}\sigma_M(w_{ME}E_i - \theta_M) \qquad i = 1, \dots, n$$

$$\sigma_M(v) = \frac{1}{1+e^{-k_M v}}$$

where x is the segmental boundary position, m is mass, F is viscoelastic force, F_M is tension force, τ_M is time relaxation constant for tension, w_{ME} is connection weight from excitatory unit to tension actuator, θ_M is threshold for tension, and k_M is the gain in function $\sigma_M(v)$, and n is the total number of segments, equal to 10. x_0 is the position of the head and x_{10} is the position of the tail. To model the piston phase, where the head and tail move concurrently, the posterior and anterior ends share the same velocity during crawling, as $\dot{x}_0 = \dot{x}_n$, which is inferred from the third equation above. Each mass block is dependent on joint force from SLS modules, tensions, and friction. Joint force from the SLS unit is affected by the segmental displacement, and tension force is regulated by the sigmoid function with gain k_t. The periodic tension force, modelled by the sigmoid function of excitatory inputs with gain k_t, is indispensable to sustain the propagation of contraction wave, which has been verified by the experimental results (Inada et al., 2011).

As for the friction force, it exists during the interaction of the mechanical body with the substrate. In this work, the transition process from static to dynamic friction is not modelled,

and the ratio of forward to backward friction is introduced to the model as directional asymmetric, considering the anterior-posterior polarity in denticle bands. Since the backward friction is larger than forward friction, the ratio is more than one. Friction on the segmental boundary is represented as:

$$f_i = \begin{cases} F_{i,ext} & \dot{x}_i = 0 \wedge -\mu_{bf}F_f \leq F_{i,ext} \leq F_f \\ F_f(\sigma_f(\dot{x}_i) - \mu_{bf}\sigma_f(-\dot{x}_i)) & otherwise \end{cases} \qquad i = 0,1,\dots,n$$

$$\sigma_f(v) = \frac{1}{1+e^{-k_f v}}$$

where f, F_f, μ_{bf} ($\mu_{bf} > 1$) individually represent the friction, forward friction and ratio for forward-backward friction, and $F_{i,ext}$ refers to the joint force of all the other forces. When the mass block is still and $F_{i,ext}$ does not exceed the range of forward-backward friction, the friction force f_i should be equal to $F_{i,ext}$. Otherwise, the friction is either the forward friction F_f or the backward one $\mu_{bf}F_f$.

Neuromuscular dynamics and modelling

The framework for the neural circuit is depicted as Figure 3B, where A27h is modelled in an excitatory population E and GDL is modelled in an inhibitory population I. The self-join connections such as E to E or I to I are not included in the model.

Meanwhile, the sensory feedback module is also important for wave propagation. The “mission-accomplished” model was proposed to depict its significance (Hughes and Thomas, 2007). After segmental contraction, the sensory neurons send a “successful contraction” message to the CNS, promoting both local relaxation and forward propagation (Hughes and Thomas, 2007). In *Drosophila* larvae, most proprioceptive neurons were found to be active when the segment is contracting, although one type was activated by extension (Vaadia et al., 2019). We model the proprioceptor as the sensory receptor SR to detect the segmental contraction. The SR unit was activated when the segmental length reached a threshold length $L\theta_S$, where L is a basal segment length (0.4 mm) and θ_S is a threshold parameter. Then it projected an inhibitory signal to the excitatory module, in order to stop muscles tightening and facilitate forward signal modelling the “mission-accomplished” role. To ensure

the sustained peristalsis, the neural connection follows the same rule between anterior and posterior terminals. The integrated neuromechanical model is shown as Figure 3C.

Under these assumptions, neural dynamics of neural circuits with EI feedforward chain are depicted based on the Wilson-Cowan model (Negahbani et al., 2015; Wilson and Cowan, 1972).

$$\begin{cases} \tau_E \dot{E}_i = -E_i + \sigma_E\left(w_{EId}\dot{I}_i + w_{EI}I_i + w_{ES}S_i - \theta_E\right) & i = 1, \dots, n-1 \\ \tau_I \dot{I}_i = -I_i + \sigma_I(w_{IE}E_{i+1} - \theta_I) & i = 1, \dots, n-1 \\ \tau_E \dot{E}_n = -E_n + \sigma_E\left(w_{EId}\dot{I}_n + w_{EI}I_n + w_{ES}S_n + ini - \theta_E\right) \\ \tau_I \dot{I}_n = -I_n + \sigma_I(w_{IE}E_1 - \theta_I) \end{cases}$$

$$S_i = \sigma_S(L\theta_S - x_{i-1} + x_i) \qquad i = 1, \dots, n$$

$$\sigma_E(v) = \frac{1}{1+e^{-k_E v}}, \qquad \sigma_I(v) = \frac{1}{1+e^{-k_I v}}, \qquad \sigma_S(v) = \frac{1}{1+e^{-k_S v}}$$

where E and I are the mean firing rates of the excitatory and inhibitory population, τ is the relaxation time constant in the EI population, w_{ab} is their synaptic connection weight from population b to population a, θ is the activation threshold of the EI population, k is its sigmoid gain and S is the feedback strength from the sensory receptor SR. The circuit includes excitatory connection via w_{IE}, w_{ME} and inhibitory connection via w_{ES}, w_{EI}. In addition to the inhibitory effect of I units, we modelled a rebound property of inhibitory synapses on excitatory neurons. Since the decline of the inhibitory inputs can be followed by the depolarization of the downstream excitatory neurons (Fushiki et al., 2016; Zwart et al., 2016), we added a term for the rebound property as a product of the time derivative of I and a weight w_{ENd} of a negative value. When the segmental length becomes smaller than the threshold $L\theta_S$, the SR unit starts to be activated. To trigger the initial crawling, we introduced an external stimulus ini, a rectangular pulse (for 5 ms), on the excitatory population in the posterior terminal.

The values of the parameters are listed in the Supplementary Table 1. All the simulation work is performed using stiff solver ode15s in MATLAB R2020a.

Acknowledgement

We thank Dr. Cengiz Pehlevan for providing MATLAB codes for reference and critical reading of the paper. This work was supported by MEXT/JSPS KAKENHI grants (22115002, 15H04255, 221S0003 to A.N. and 26430004, 17K07042, 217D0344 to H.K.).

Competing interests

We have no conflict of interest with respect to the work.

References

Aguilar J, Zhang T, Qian F, Kingsbury M, McInroe B, Mazouchova N, Li C, Maladen R, Gong C, Travers M, Hatton RL, Choset H, Umbanhowar PB, Goldman DI. 2016. A review on locomotion robophysics: The study of movement at the intersection of robotics, soft matter and dynamical systems. *Reports Prog Phys* **79**. doi:10.1088/0034-4885/79/11/110001

Banks HT, Hu S, Kenz ZR. 2011. A brief review of elasticity and viscoelasticity for solids. *Adv Appl Math Mech* **3**:1–51. doi:10.4208/aamm.10-m1030

Berni J. 2015. Genetic dissection of a regionally differentiated network for exploratory behavior in drosophila larvae. *Curr Biol* **25**:1319–1326. doi:10.1016/j.cub.2015.03.023

Berrigan D, Pepin DJ. 1995. How maggots move: Allometry and kinematics of crawling in larval Diptera. *J Insect Physiol* **41**:329–337. doi:10.1016/0022-1910(94)00113-U

Clark MQ, Zarin AA, Carreira-Rosario A, Doe CQ. 2018. Neural circuits driving larval locomotion in Drosophila. *Neural Dev*. doi:10.1186/s13064-018-0103-z

Corucci F, Cheney N, Giorgio-Serchi F, Bongard J, Laschi C. 2018. Evolving soft locomotion in aquatic and terrestrial environments: Effects of material properties and

environmental transitions. *Soft Robot* **5**:475–493. doi:10.1089/soro.2017.0055

Daun S, Rubin JE, Rybak IA. 2009. Control of oscillation periods and phase durations in half-center central pattern generators: A comparative mechanistic analysis. *J Comput Neurosci* **27**:3–36. doi:10.1007/s10827-008-0124-4

Fox LE, Soll DR, Wu CF. 2006. Coordination and modulation of locomotion pattern generators in Drosophila larvae: Effects of altered biogenic amine levels by the tyramine β hydroxlyase mutation. *J Neurosci* **26**:1486–1498. doi:10.1523/JNEUROSCI.4749-05.2006

Fushiki A, Zwart MF, Kohsaka H, Fetter RD, Cardona A, Nose A. 2016. A circuit mechanism for the propagation of waves of muscle contraction in Drosophila. *Elife* **5**:1–23. doi:10.7554/eLife.13253

Garrity PA, Goodman MB, Samuel AD, Sengupta P. 2010. Running hot and cold: Behavioral strategies, neural circuits, and the molecular machinery for thermotaxis in C. elegans and Drosophila. *Genes Dev*. doi:10.1101/gad.1953710

Gjorgjieva J, Berni J, Evers JF, Eglen SJ. 2013. Neural circuits for peristaltic wave propagation in crawling drosophila larvae: Analysis and modeling. *Front Comput Neurosci*. doi:10.3389/fncom.2013.00024

Green CH, Burnet B, Connolly KJ. 1983. Organization and patterns of inter- and intraspecific variation in the behaviour of Drosophila larvae. *Anim Behav* **31**:282–291. doi:10.1016/S0003-3472(83)80198-5

Green N, Odell N, Zych M, Clark C, Wang ZH, Biersmith B, Bajzek C, Cook KR, Dushay MS, Geisbrecht ER. 2016. A common suite of coagulation proteins function in drosophila muscle attachment. *Genetics* **204**:1075–1087. doi:10.1534/genetics.116.189787

Heckscher ES, Lockery SR, Doe CQ. 2012. Characterization of Drosophila larval crawling at the level of organism, segment, and somatic body wall musculature. *J Neurosci* **32**:12460–12471. doi:10.1523/JNEUROSCI.0222-12.2012

Heckscher ES, Zarin AA, Faumont S, Clark MQ, Manning L, Fushiki A, Schneider-Mizell CM, Fetter RD, Truman JW, Zwart MF, Landgraf M, Cardona A, Lockery SR, Doe CQ. 2015. Even-Skipped+ Interneurons Are Core Components of a Sensorimotor Circuit that Maintains Left-Right Symmetric Muscle Contraction Amplitude. *Neuron* **88**:314–329. doi:10.1016/j.neuron.2015.09.009

Hughes CL, Thomas JB. 2007. A sensory feedback circuit coordinates muscle activity in Drosophila. *Mol Cell Neurosci* **35**:383–396. doi:10.1016/j.mcn.2007.04.001

Inada K, Kohsaka H, Takasu E, Matsunaga T, Nose A. 2011. Optical dissection of neural circuits responsible for drosophila larval locomotion with Halorhodopsin. *PLoS One* **6**:e29019. doi:10.1371/journal.pone.0029019

Itakura Y, Kohsaka H, Ohyama T, Zlatic M, Pulver SR, Nose A. 2015. Identification of Inhibitory Premotor Interneurons Activated at a Late Phase in a Motor Cycle during Drosophila Larval Locomotion. *PLoS One* **10**:e0136660. doi:10.1371/journal.pone.0136660

Kakanj P, Eming SA, Partridge L, Leptin M. 2020. Long-term in vivo imaging of Drosophila larvae. *Nat Protoc* 1–30. doi:10.1038/s41596-019-0282-z

Kim S, Laschi C, Trimmer B. 2013. Soft robotics: A bioinspired evolution in robotics. *Trends Biotechnol* **31**:287–294. doi:10.1016/j.tibtech.2013.03.002

Kohsaka H, Guertin PA, Nose A. 2017. Neural Circuits Underlying Fly Larval Locomotion. *Curr Pharm Des* **23**:1722–1733. doi:10.2174/1381612822666161208120835

Kohsaka H, Okusawa S, Itakura Y, Fushiki A, Nose A. 2012. Development of larval motor

circuits in Drosophila. *Dev Growth Differ* **54**:408–419. doi:10.1111/j.1440-169X.2012.01347.x

Kohsaka H, Takasu E, Morimoto T, Nose A. 2014. A group of segmental premotor interneurons regulates the speed of axial locomotion in drosophila larvae. *Curr Biol* **24**:2632–2642. doi:10.1016/j.cub.2014.09.026

Lahiri S, Shen K, Klein M, Tang A, Kane E, Gershow M, Garrity P, Samuel ADT. 2011. Two alternating motor programs drive navigation in Drosophila larva. *PLoS One* **6**:e23180. doi:10.1371/journal.pone.0023180

Lin HT, Dorfmann AL, Trimmer BA. 2009. Soft-cuticle biomechanics: A constitutive model of anisotropy for caterpillar integument. *J Theor Biol* **256**:447–457. doi:10.1016/j.jtbi.2008.10.018

Louis M, Huber T, Benton R, Sakmar TP, Vosshall LB. 2008. Bilateral olfactory sensory input enhances chemotaxis behavior. *Nat Neurosci* **11**:187–199. doi:10.1038/nn2031

Loveless J, Lagogiannis K, Webb B. 2019. Modelling the mechanics of exploration in larval Drosophila. *PLoS Comput Biol* **15**. doi:10.1371/journal.pcbi.1006635

Luo L, Gershow M, Rosenzweig M, Kang KJ, Fang-Yen C, Garrity PA, Samuel ADT. 2010. Navigational decision making in Drosophila thermotaxis. *J Neurosci* **30**:4261–4272. doi:10.1523/JNEUROSCI.4090-09.2010

Matsunaga T, Fushiki A, Nose A, Kohsaka H. 2013. Optogenetic perturbation of neural activity with laser illumination in semi-intact drosophila larvae in motion. *J Vis Exp* e50513–e50513. doi:10.3791/50513

Negahbani E, Steyn-Ross DA, Steyn-Ross ML, Wilson MT, Sleigh JW. 2015. Noise-Induced Precursors of State Transitions in the Stochastic Wilson–Cowan Model. *J Math Neurosci* **5**:1–27. doi:10.1186/s13408-015-0021-x

Nishikawa K, Biewener AA, Aerts P, Ahn AN, Chiel HJ, Daley MA, Daniel TL, Full RJ, Hale ME, Hedrick TL, Lappin AK, Nichols TR, Quinn RD, Satterlie RA, Szymik B. 2007. Neuromechanics: An integrative approach for understanding motor control. *Integr Comp Biol* **47**:16–54. doi:10.1093/icb/icm024

Paoletti P, Mahadevan L. 2014. A proprioceptive neuromechanical theory of crawling. *Proc R Soc B Biol Sci* **281**. doi:10.1098/rspb.2014.1092

Paterson BA, Marko Anikin I, Krans JL. 2010. Hysteresis in the production of force by larval Dipteran muscle. *J Exp Biol* **213**:2483–2493. doi:10.1242/jeb.043026

Pehlevan C, Paoletti P, Mahadevan L. 2016. Integrative neuromechanics of crawling in D. Melanogaster Larvae. *Elife* **5**. doi:10.7554/eLife.11031

Quillin K. 1998. Ontogenetic scaling of hydrostatic skeletons: geometric, static stress and dynamic stress scaling of the earthworm lumbricus terrestris. *J Exp Biol* **201**.

Quillin KJ. 1999. Kinematic scaling of locomotion by hydrostatic animals: ontogeny of peristaltic crawling by the earthworm lumbricus terrestris. *J Exp Biol* **202**.

Repiso A, Saavedra P, Casal J, Lawrence PA. 2010. Planar cell polarity: The orientation of larval denticles in Drosophila appears to depend on gradients of Dachsous and Fat. *Development* **137**:3411–3415. doi:10.1242/dev.047126

Ross D, Lagogiannis K, Webb B. 2015. A model of larval biomechanics reveals exploitable passive properties for efficient locomotion. *Lect Notes Comput Sci (including Subser Lect Notes Artif Intell Lect Notes Bioinformatics)* **9222**:1–12. doi:10.1007/978-3-319-22979-9_1

Schindelin J, Arganda-Carreras I, Frise E, Kaynig V, Longair M, Pietzsch T, Preibisch S, Rueden C, Saalfeld S, Schmid B, Tinevez JY, White DJ, Hartenstein V, Eliceiri K, Tomancak P, Cardona A. 2012. Fiji: An open-source platform for biological-image

analysis. *Nat Methods*. doi:10.1038/nmeth.2019

Takagi S, Cocanougher BT, Niki S, Miyamoto D, Kohsaka H, Kazama H, Fetter RD, Truman JW, Zlatic M, Cardona A, Nose A. 2017. Divergent Connectivity of Homologous Command-like Neurons Mediates Segment-Specific Touch Responses in Drosophila. *Neuron* **96**:1373-1387.e6. doi:10.1016/j.neuron.2017.10.030

Trivedi D, Rahn CD, Kier WM, Walker ID. 2008. Soft robotics: Biological inspiration, state of the art, and future research. *Appl Bionics Biomech* **5**:99–117. doi:10.1080/11762320802557865

Trueman ER (Edwin R. 1975. The locomotion of soft-bodied animals. Edward Arnold.

Tytell ED, Holmes P, Cohen AH. 2011. Spikes alone do not behavior make: Why neuroscience needs biomechanics. *Curr Opin Neurobiol* **21**:816–822. doi:10.1016/j.conb.2011.05.017

Vaadia RD, Li W, Voleti V, Singhania A, Hillman EMC, Grueber WB. 2019. Characterization of Proprioceptive System Dynamics in Behaving Drosophila Larvae Using High-Speed Volumetric Microscopy. *Curr Biol* **29**:935-944.e4. doi:10.1016/j.cub.2019.01.060

Wallace HR. 1969. Wave formation by infective larvae of the plant parasitic nematode meloidogyne javanica. *Nematologica*. doi:10.1163/187529269X00100

Wilson HR, Cowan JD. 1972. Excitatory and Inhibitory Interactions in Localized Populations of Model Neurons, Biophysical Journal. doi:10.1016/S0006-3495(72)86068-5

Yoshikawa S, Long H, Thomas JB. 2016. A subset of interneurons required for Drosophila larval locomotion. *Mol Cell Neurosci* **70**:22–29. doi:10.1016/j.mcn.2015.11.008

Zarin AA, Mark B, Cardona A, Litwin-Kumar A, Doe CQ. 2019. A Drosophila larval premotor/motor neuron connectome generating two behaviors via distinct spatio-temporal muscle activity. *bioRxiv* 617977. doi:10.1101/617977

Zwart MF, Pulver SR, Truman JW, Fushiki A, Fetter RD, Cardona A, Landgraf M. 2016. Selective Inhibition Mediates the Sequential Recruitment of Motor Pools. *Neuron* **91**:615–628. doi:10.1016/j.neuron.2016.06.031

Supplementary material

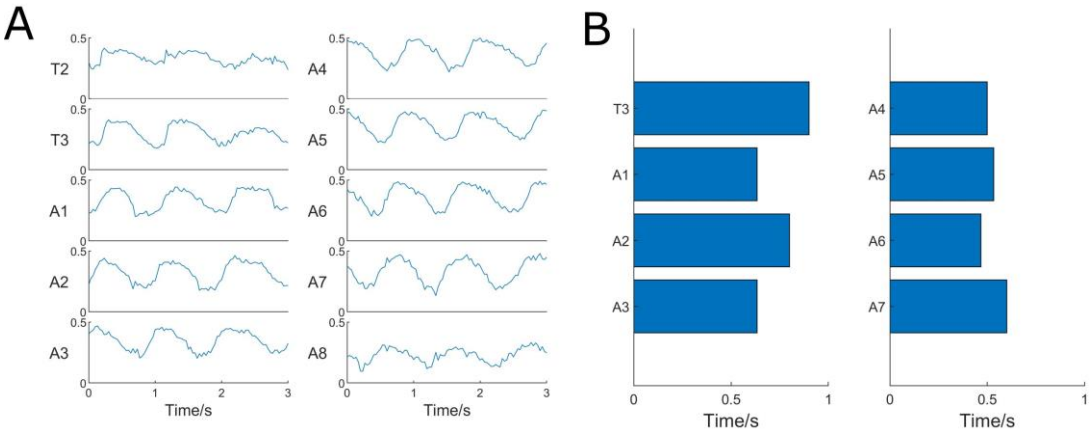

Supplementary Figure 1. Segmental dynamics of 3rd instar larva, correlated to Figure 1. (A) Segmental length change measured in crawling larvae. The lengths are normalized by the maximum length of each segment. (B) The contraction duration of each segment in crawling larvae.

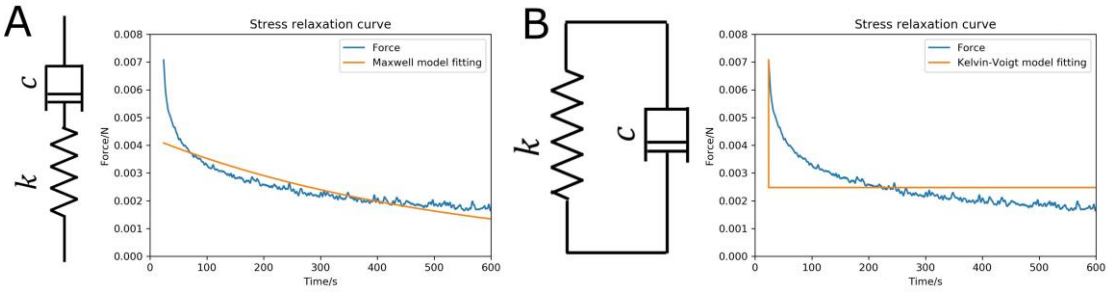

Supplementary Figure 2. Fitting stress relaxation curves with different mechanical models. (A) (Left) the Maxwell model, (right) fitting stress relaxation data (blue) with the Maxwell model (orange). (B) (Left) the Kelvin-Voigt model, (right) fitting stress relaxation data with the Kelvin-Voigt model.

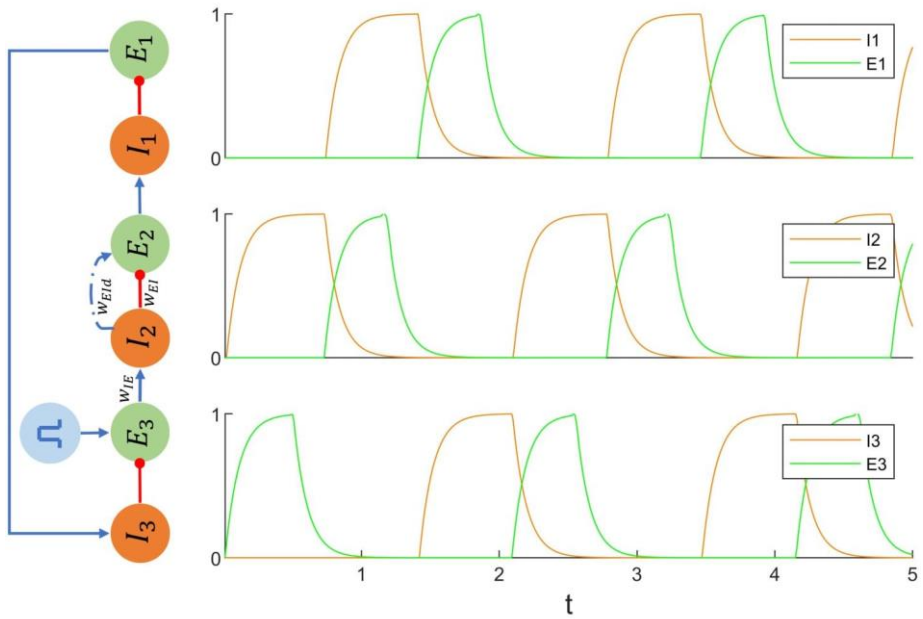

Supplementary Figure 3. Neural dynamics of the neural chain model. (Left) The connection map of the neural chain of excitatory (E_i) and inhibitory (I_i) units with three segments. (Right) traces of activity of excitatory and inhibitory units in the simulation. Initial pulse stimuli are applied to the E_3unit as shown.

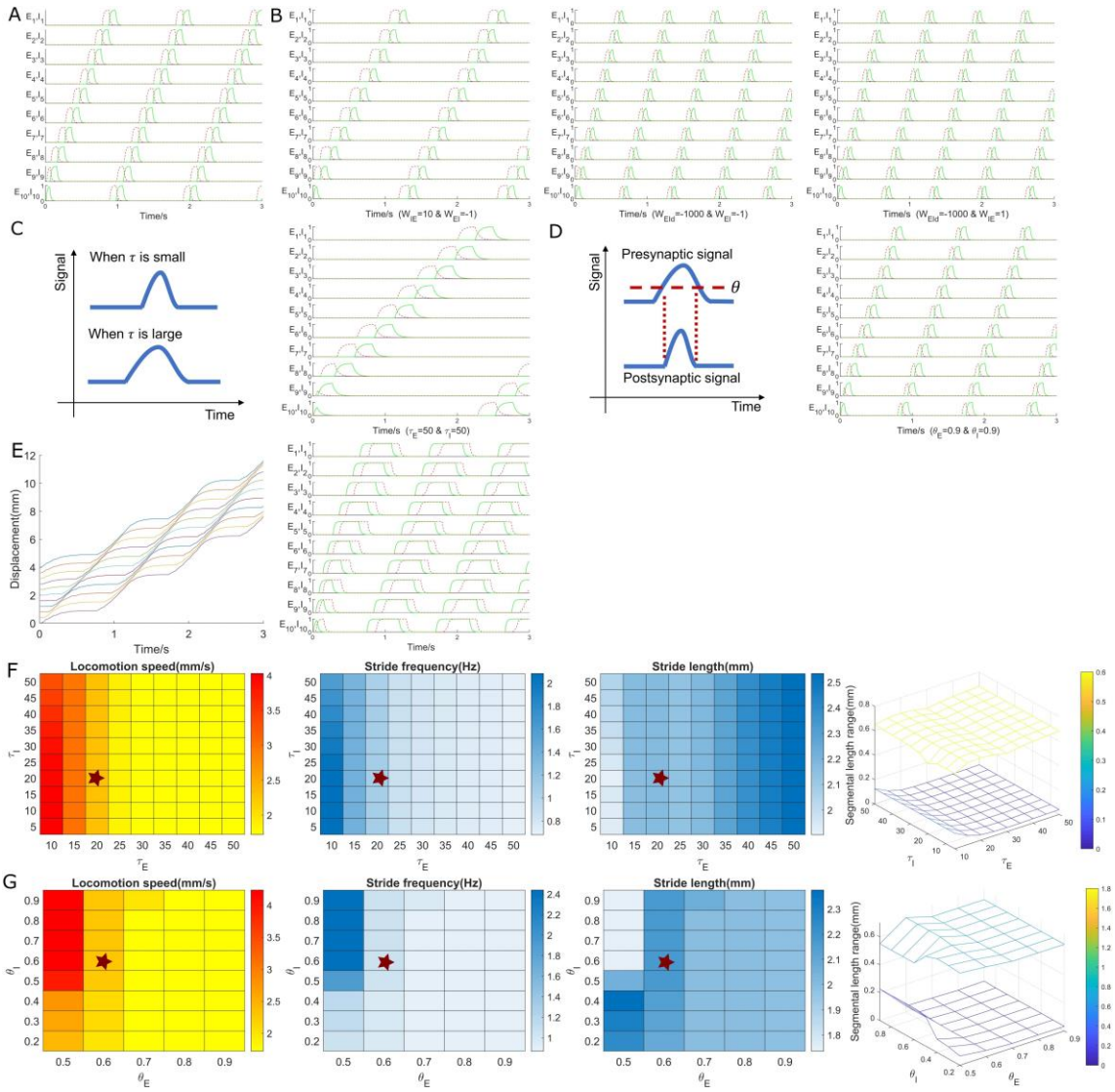

Supplementary Figure 4. Kinematic analysis of the effect of neural circuit parameters. (A) Neural dynamics with the default configuration of the parameters. (B) Neural dynamics in large w_{IE} (left) and small w_{EId} (middle and right). (C and D) (Left) sketch of an effect of parameters (time relaxation constant τ and threshold θ), (right) neural dynamics when these parameters are large. (E) Locomotion and neural dynamics referring to the neural circuit framework described in Pehlevan et al., (2016)**.** (F and G) Responses of locomotion speed, stride frequency and segmental dynamics with perturbations of neural parameters. (All the stars in F and G refer to the default configurations of parameters in the neuromechanical model; the connection weights follow the original configurations.)

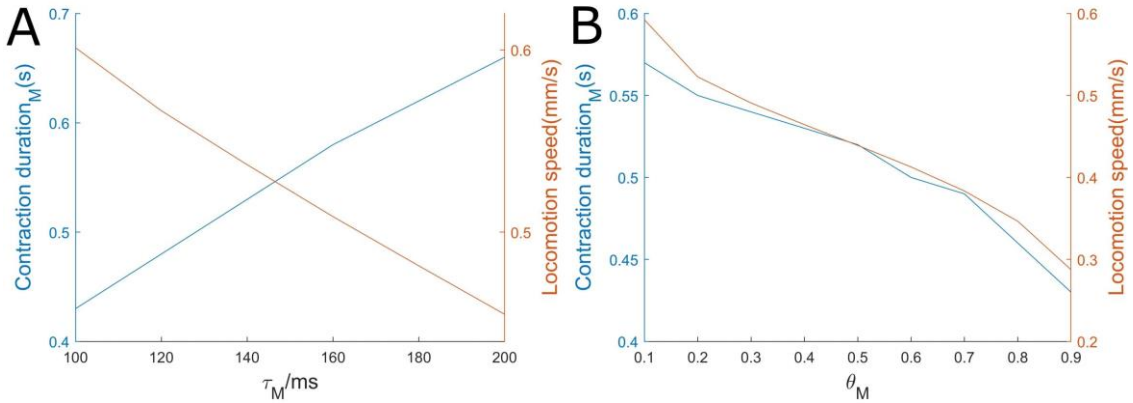

Supplemental Figure 5. Kinematic analysis of the effect of muscle contraction parameters. (A) Responses of the muscle contraction duration and locomotion speed in the perturbation of time relaxation constant τ_t in muscles. (B) Responses of the muscle contraction duration and locomotion speed in the perturbation of the threshold of muscle contraction θ_t.

Supplementary Table 1. Parameters for the simulation of the neuromechanical model and their default configurations.

Symbol	Value	Symbol	Value
m	0.1 mg	L	0.4 mm
k_1	3 mg/msec^2	k_2	3 mg/msec^2
$\boldsymbol{c}$	475000 mg/msec	t_{max}	4 mN
Ff	0.05 mN	μ_{bf}	10
w_{EI}	-1	w_{EId}	-10000
w_{IE}	1	w_{ES}	-1
w_{tE}	1	θ_E	0.5
θ_I	0.5	θ_t	0.2
θ_S	0.8	τ_E	15 ms
τ_I	15 ms	τ_t	150 ms

Supplementary Video 1. Larval crawling, with fluorescent segmental labels. The genotype is *tubP-Gal4, UAS-fondue::GFP*. The transgenes label the muscle attachment sites and visualize segmental boundaries.

Supplementary Video 2. Larval crawling with labels in the abdominal segments when floated on 66% sugar solution. The genotype is *R70C01-Gal4, UAS-CD4::GFP*. The transgenes label oenocytes, which are located at every segment.